Engineering Applications of Computational Fluid Mechanics Vol. 8, No. 3, pp. 356-372 (2014)

NUMERICAL PREDICTION OF PARTICLE DISTRIBUTION OF SOLID-LIQUID SLURRIES IN STRAIGHT PIPES AND BENDS

Gianandrea Vittorio Messa* and Stefano Malavasi

Dipt. I.C.A., Piazza Leonardo da Vinci, 32, 20133 Milano, Italy
**E-Mail: gianandreavittorio.messa@polimi.it (Corresponding Author)*

ABSTRACT: Turbulent solid-liquid slurry flows in pipes are encountered in many engineering fields, such as mining. In particular, the distribution of the solids is a serious concern to engineers, but its determination involves considerable technical and economic difficulties. A two-fluid model for the numerical prediction of this parameter is presented. The model is robust and numerically stable, and requires relatively short computer time to provide a converged steady-state solution. The novelty of the proposed model and its better performance compared to similar ones reside in the method of accounting for some key physical mechanisms governing these flows, namely turbulent dispersion, interphase friction, and viscous and mechanical contributions to friction. The model is first validated by comparison with many experimental data available in literature regarding the horizontal pipe case over a wide range of operating conditions: delivered solid volume fraction between 9 and 40%; slurry velocity between 1 m/s and 5.5 m/s; and pipe diameter between 50 and 160 mm. A further comparison was performed with respect to recent experiments concerning a horizontal 90° bend.

Keywords: two-fluid model, numerical analysis, slurries, two-phase flow, horizontal pipes, pipe bends

1. INTRODUCTION

Pipe flows of solid-liquid mixtures in the form of slurry are commonly encountered in many applications. A significant example is given by the slurry pipelines, used to transport mineral concentrate from a mineral processing plant near a mine. Pressure gradient and concentration distribution have been the most serious concern of researchers, as they dictate the selection of pump capacity and may be used to determine parameters of direct importance (mixture and solid flow rates) as well as secondary effects like wall abrasion and particle degradation.

The flow of solid-liquid mixtures is very complex. Doron and Barnea (1996) identified the flow patterns that characterize the flow of slurries through horizontal pipes. If the flow rate is sufficiently high, turbulence is effective in keeping all the solids suspended (fully suspended flow); otherwise the particles accumulate at the pipe bottom and form a packed bed, either sliding (flow with a moving bed) or not (flow with a stationary bed). The transitions between flow patterns are not always so clear and they are usually identified by post-processing analysis of the measured data in terms of solid volume fraction profile and pressure gradient (Albunaga, 2002).

Numerous experimental investigations have been carried out to determine the main features of slurry flows in pipes. Almost all of them concern the case of horizontal pipes; the dispersed phase is usually sand (Roco and Shook, 1983; Colwell and Shook, 1988; Shaan et al., 2000; Matousek, 2000 and 2002; Gillies et al., 2004; Skudarnov et al., 2004; Kim et al., 2008), but spherical glass beads (Kaushal and Tomita, 2003 and 2007; Kaushal et al., 2005 and 2012), ash (Kumar et al., 2003), and solid nitrogen particles (Jiang and Zhang, 2012) have also been considered. Only few studies were focused on vertical pipes (Shook and Bartosik, 1994) and bends (Hsu, 1981; Turian et al., 1998; Kaushal et al., 2013). The distribution of the solids is very hard to determine experimentally. Local values of solid volume fraction can be measured by isokinetic probe sampling, but these techniques may produce significant errors near both the pipe wall (Nasr-el-Din et al., 1984) and the pipe axis (Colwell and Shook, 1988). More accurate results – but with uncertainties of a few percent – are obtained using expensive gamma-ray density gauges, which are used to determine chord-average values of solids concentration. The mean volumetric concentration of the slurry is characterized in different ways by researchers. Kaushal and Tomita (2003 and 2007) and Kaushal et al. (2005) considered an overall-area average concentration, evaluated by integrating the local concentration profile measured by an isokinetic sampling probe. Matousek (2000 and 2002) measured the delivered solid volume

Received: 31 Jan. 2013; Revised: 25 Feb. 2014; Accepted: 5 Mar. 2014

fraction in the pipeline by a counter flow meter. Other authors (Shaan et al., 2000; Gillies et al., 2004) have made reference to a mean in-situ volume fraction, obtained by adding weighted quantities of solids to the loop, whose volume was known. In all cases, the uncertainty about this parameter must be considered when making reference to literature data.

In the past simplified models have been developed based on a global formulation to predict the pressure gradient of slurries in horizontal pipes for all the flow configurations: equivalent liquid models for fully-suspended flow (Matousek, 2002; Pecker and Helvaci, 2008), two-layer models for flows with a moving bed (Gillies and Shook, 2000; Gillies et al., 2004; Doron et al., 1987), three layer models for flows with a stationary deposit (Doron and Barnea, 1993 and 1995; Matousek, 2009). Improved versions have been proposed to account for the presence of multi-sized particles (Kumar et al., 2003), the influence of particle shape (Shaan et al., 2000), the additional stresses due to particle-wall interactions (Pecker and Helvaci, 2008), and the repulsion of particles from the wall observed under certain conditions (Wilson et al., 2010). Using those models, the major losses in horizontal pipes can be estimated easily and the predictions agree with the experimental evidence over a wide range of operating conditions. Therefore, these models represent a very powerful tool for most engineering applications. However, their global formulation makes them unsuitable for predicting the solids concentration distribution as well as for application to more complex flows; meeting these needs requires the development and validation of distributed models.

CFD has been used to investigate slurry flows in pipes, mostly with regard to the horizontal pipe case. Anyway, the development of a model that is both reliable over a wide range of flow conditions and computationally economical – therefore attractive to engineers – is a goal which has not been completely reached yet.

The majority of existing CFD models employs an Eulerian-Eulerian approach, since Eulerian-Lagrangian models are not applicable to dense mixtures due to their excessive computational cost. Some workers studied the problem by means of the Algebraic Slip Model (ASM), which solves the momentum equation for the mixture rather than for both phases, thereby saving computational time. However, the ASM assumes that local equilibrium is achieved between the phases over short spatial length scales. Therefore, it can be used only for very low values of the Stokes number. Also when applicable, the ASM proved inadequate to estimate the pressure drop even for fully-suspended flows in straight pipes (Kaushal et al., 2012), and it does not seem very accurate in predicting the solid volume fraction distribution (Ling et al., 2003; Kaushal et al., 2012; Pathak, 2011).

Other authors made use of an Eulerian two-fluid model with closures derived either from empirical or semi-empirical relations (Chen, 1994), or from kinetic theory of granular flow (KTGF) (Chen et al., 2009; Ekambara et al., 2009; Lahiri and Ghanta, 2010; Kaushal et al., 2012 and 2013). Anyway, even for straight pipe flows, the existing two-fluid models show some problems which may complicate their application to more complex flows of engineering interest, such as those through bends and pipeline fittings. The first impression is that these models are easily susceptible to numerical instabilities, which often result in solutions characterized by non-physical asymmetry (Kaushal et al., 2012) or oscillations (Lahiri and Ghanta, 2010). In some cases, the simulations are very time-consuming; for example, Ekambara and co-workers (2009) attained a stable steady-state solution performing a U-RANS simulation and then averaged the solution over a considerable time interval. A similar procedure may not be easily applicable when dealing with complex geometries, since the calculation time would probably become prohibitively expensive. In other cases, the validation of these models with respect to the experimental evidence is often rather poor, in the sense that the comparison is either limited to a few flow conditions (Chen et al., 2009; Kaushal et al., 2012) or highlights a occasionally excellent capacity of the model to describe adequately the main features of the flow (Lahiri and Ghantha, 2010).

Within the flow conditions commonly encountered in slurry pipelines, the recent work of Kaushal et al. (2013) seems the only application of a two-fluid model to a more complex flow configuration (i.e. through a 90° bend in a horizontal pipe), with the predictions compared with experimental data.

In the present work a mathematical model is presented for the numerical prediction of the particle distribution of solid-liquid slurry flows in pipes, which is based on an Euler-Euler approach that uses the Inter-Phase Slip Algorithm (IPSA) of Spalding (1980). The proposed model shows comparable or better agreement with the experimental evidence than similar models (Ekambara et al., 2009; Lahiri and Ghanta, 2010;

Kaushal et al., 2012 and 2013), and it also overcomes the main limitations inferred from inspection of these earlier papers, namely susceptibility to numerical instability and high computational cost. In fact, the new model requires relatively short computer time to attain a converged steady-state solution and is capable of providing a numerical solution without non-physical asymmetries or oscillations. The novelty of the proposed model, which is the basis for its good performance, resides in the combined use of modelling strategies previously developed but never employed simultaneously to the flows considered in this paper: phase diffusion fluxes are introduced in all conservation equations to reproduce the effect of the turbulent dispersion of particles; the presence of other particles on the interfacial momentum transfer is taken into account by considering their effect on a mixture viscosity; a wall function is employed to model the viscous (due to the fluid) and mechanical (due to the particles) contributions to the wall shear stress. The model is considerably simpler and solves one transport equation fewer than those based on the KTGF.

In the interests of guaranteeing the widest possible applicability, the model predictions of the concentration distribution are validated with respect to various sets of experimental data from the literature. The measurements from Roco and Shook (1983), Shaan et al. (2000), Matousek (2000 and 2002), and Gillies et al. (2004) allow establishing the predictive capacity of the model in the horizontal pipe case over different flow configurations (fully-suspended flow, and flow with a moving bed) and a large range of operating conditions: delivered solid volume fraction between 9 and 40%; particle size between 90 and 520 μm; slurry velocity between 1 m/s and 5.5 m/s; pipe diameter between 50 and 160 mm. Finally, the model was applied to a more complex flow, which is that through a 90° bend in a horizontal pipe, and the predictions were successfully compared with the experiments from Kaushal et al. (2013). The uncertainties of both computations and measurements are discussed when comparing the numerical results with experimental data.

2. MATHEMATICAL MODEL

2.1 Conservation equations

The two-phase flow is represented by using an Eulerian approach in which both phases are treated as interpenetrating continua. The flow is assumed to be statistically steady in the sense that Reynolds-averaging has been applied and so the continuity equation for phase $k = C, p$ takes the following form:

$$\nabla \cdot \left(\alpha_k \rho_k \mathbf{U}_k \right) = \nabla \cdot \left(\rho_k D \nabla \alpha_k \right) \tag{1}$$

where the subscript k is a phase indicator parameter which is equal to C for the carrier fluid and p for the particles. Moreover α_k is the volume fraction; ρ_k is the density; $\mathbf{U}_k$ is the velocity vector; and D is a phase diffusion coefficient, which appears in the phase diffusion term that represents the turbulent flux associated with correlations between fluctuating velocity and volume fraction. The phase diffusion fluxes are modeled in terms of a gradient diffusion approximation with the phase-diffusion coefficient D given by:

$$D = \frac{\nu_{t,C}}{\sigma_\alpha} \tag{2}$$

where $\nu_{t,C}$ is the turbulent kinematic viscosity of the carrier fluid phase, determined by turbulence modeling; and σ_α is the turbulent Schmidt number for volume fractions. The turbulent Schmidt number for volume fractions is not well established, in the sense that no single constant value of σ_α can be used in the numerical simulations to match the various sets of experimental data (Shirolkar et al., 1996), but rather previous workers (Chen, 1994; Chen et al., 2011) have found that different constant values are needed for different cases. These values typically fall in the range of 0.2 to 0.9. In the present work, a constant value was used in the simulations, and as will be discussed later, the choice of a unique value procured good overall agreement with the various sets of experimental data. The presence of phase diffusion fluxes in all conservation equations, which has the advantage of promoting numerical stability, distinguishes the present model from similar ones applied to slurry flows. The mean global continuity is given by the equation that states that the two volume fractions must sum to unity.

The momentum equation for phase $k = C, p$ is:

$$\begin{aligned} &\nabla \cdot \left(\alpha_k \rho_k \mathbf{U}_k \mathbf{U}_k \right) \\ &= -\alpha_k \nabla P + \nabla \cdot \left[\alpha_k \left(\boldsymbol{T}_{v,k} + \boldsymbol{T}_{t,k} \right) \right] + \alpha_k \rho_k \mathbf{g} \\ &\quad + \mathbf{M}_k + \nabla \cdot \left(\rho_k D \mathbf{U}_k \nabla \alpha_k \right) \end{aligned} \tag{3}$$

where P is the pressure, shared by the phases; $\mathbf{g}$ is the gravitational acceleration; $\boldsymbol{T}_{v,k}$ and $\boldsymbol{T}_{t,k}$ are the viscous and turbulent stress tensors respectively; and $\mathbf{M}_k$ is the generalized drag force per unit volume, which will be discussed later.

The stress tensors are given by:

$$\boldsymbol{T}_{\nu,k} = 2\rho_k \nu_{l,k} \boldsymbol{D}_k, \qquad \boldsymbol{T}_{t,k} = 2\rho_k \nu_{t,k} \boldsymbol{D}_k \tag{4}$$

where $\nu_{l,k}$ and $\nu_{t,k}$ are the laminar and turbulent kinematic viscosity of phase k respectively, and $\boldsymbol{D}_k$ is the deformation tensor, equal to:

$$\boldsymbol{D}_k = 0.5\left[\nabla \mathbf{U}_k + (\nabla \mathbf{U}_k)^+\right] \tag{5}$$

where the superscript "+" indicates that the transpose of the dyadic $\nabla \mathbf{U}_k$ is taken.

Two viscosities appear in Eq. (4) for the particle phase, namely, the turbulent eddy viscosity $\nu_{t,p}$, and the laminar viscosity $\nu_{l,p}$. The former is determined from a turbulence model, as will be discussed later. The latter is commonly associated with the inter-granular stresses which characterize bed flows (Chen et al., 2011); the model of Ahilan and Sleath (1987) for $\nu_{l,p}$ was briefly explored but finally $\nu_{l,p}$ was set to 0 after discovering the negligible influence of the term $\boldsymbol{T}_{\nu,p}$ on the predictions of the solids volume fraction for all the flow conditions simulated. This can be explained by the fact that the laminar viscosity of the particles is small compared to the eddy viscosity, except very close to the pipe bottom, where however, the interfacial momentum transfer term dominates.

The interfacial momentum transfer term accounts for the momentum transfer between phases, and is given by stationary drag, lift, added mass, history and other forces (Ishii and Mishima, 1984). The two-fluid model represents the turbulent dispersion of particles by means of a turbulent diffusion term in the phasic continuity equation (Eq. (1)), and so an explicit turbulent-dispersion force term does not appear in the momentum equation. A literature review revealed that the history force is negligible for the flows considered here (Chung and Troutt, 1988), and therefore was not included in this model. Under the assumption of mono-dispersed spherical particles, the interfacial momentum transfer term is given by:

$$\mathbf{M}_C = -\mathbf{M}_p = \frac{6\alpha_p}{\pi d_p^3}\left(\mathbf{F}_d + \mathbf{F}_l + \mathbf{F}_{vm}\right) \tag{6}$$

where $\mathbf{F}_d$, $\mathbf{F}_l$, and $\mathbf{F}_{vm}$ are the drag, lift, and virtual mass forces, calculated respectively as follows:

$$\mathbf{F}_d = \frac{1}{2}\left(\pi \frac{d_p^2}{4}\right) C_d \rho_C \left|\mathbf{U}_p - \mathbf{U}_C\right| \left(\mathbf{U}_p - \mathbf{U}_C\right) \tag{7}$$

$$\mathbf{F}_l = C_l \rho_C d_p^3 \left(\mathbf{U}_p - \mathbf{U}_C\right) \times \left(\nabla \times \mathbf{U}_C\right) \tag{8}$$

$$\mathbf{F}_{vm} = \left(\frac{4}{3}\pi \frac{d_p^3}{8}\right) C_{vm} \rho_C \left(\mathbf{U}_p \cdot \nabla \mathbf{U}_p - \mathbf{U}_C \cdot \nabla \mathbf{U}_C\right) \tag{9}$$

where d_p is the particle diameter; C_d is the drag coefficient, which will be discussed later; C_l is the lift coefficient; and C_{vm} is the virtual mass coefficient. As per the indications of Kaushal et al. (2012), both C_l and C_{vm} were set equal to 0.5.

The drag coefficient is given by the well known Schiller and Naumann (1935) formula:

$$C_d = \max\left[\frac{24}{\mathrm{Re}_p}\left(1 + 0.15\,\mathrm{Re}_p^{0.687}\right), 0.44\right] \tag{10}$$

in which Re_p is the particle Reynolds number. The use of alternative correlations (Clift et al., 1978; Ishii and Mishima, 1984) does not seem to have significant impact on the results, as they do not differ very much from Eq. (10) in the range of Re_p considered. Following a well-established approach (Barnea and Mizrahi, 1973; Ishii and Mishima, 1984) to account for the presence of other particles, the particle Reynolds number is defined as $\mathrm{Re}_p = \rho_C d_p |\mathbf{U}_r| / \mu_m$, where μ_m is the viscosity of the mixture. Several correlations for the mixture viscosity are available in literature (Clift el al., 1978). They are basically empirical, or semi-empirical, and they depend on parameters that account for the shape and size distribution of the particles. In the present work use is made of the Mooney (1951) formula:

$$\mu_m = \rho_C \nu_{l,C} \exp\left(\frac{[\eta]\alpha_p}{1 - \alpha_p / \alpha_{pm}}\right) \tag{11}$$

in which the two fitting parameters are the maximum packing concentration α_{pm} and the intrinsic viscosity $[\eta]$. The former accounts for the shape and size distribution of the particles, as well as the shear rate (Pecker and Helvaci, 2008); whereas the latter accounts for particle shape. For the first time, the mixture viscosity approach is employed in a two-fluid model for the simulation of slurry flows in pipes. In particular, the asymptotic behaviour of the viscosity of the mixture, which tends to infinity as the solids volume fraction approaches the maximum packing one, sets an upper limit to the concentration of particles, preventing the solids from over-packing. This avoids the need to introduce a collisional pressure term in the dispersed phase momentum equations. The absence of this term contributes to the numerical stability of the present model.

Some authors have argued for the existence of a wall lubrication force in the generalized drag term to account for the repulsion of particles from the pipe wall observed in some experiments (Matousek, 2002; Kaushal and Tomita, 2007), but this effect is not considered in the present work. A semi-theoretical model for this force was derived

by Antal et al. (1991) for air-water bubbly flow in the laminar regime, but it proved unsuitable for slurry flows, confirming the observations of Ekambara et al. (2009). Wilson and Sellgren (2003) and Wilson et al. (2010) proposed a model for the wall-lubrication force in slurry flows, but the global nature of its formulation precludes its implementation in a CFD code.

2.2 Turbulence modeling

The following modified form of the *k*-ε model is used for turbulence modeling of the fluid phase:

$$\begin{aligned}&\nabla\cdot\left(\alpha_C\rho_C\mathbf{U}_C k\right)\\&=\nabla\cdot\left[\alpha_C\rho_C\left(\nu_{l,C}+\frac{\nu_{t,C}}{\sigma_k}\right)\nabla k\right]+\alpha_C\rho_C\left(P_k-\varepsilon\right)\\&+\nabla\cdot\left[\rho_C\frac{\nu_{t,C}}{\sigma_\alpha}k\nabla\alpha_C\right]\end{aligned}\tag{12}$$

$$\begin{aligned}&\nabla\cdot\left(\alpha_C\rho_C\mathbf{U}_C\varepsilon\right)\\&=\nabla\cdot\left[\alpha_C\rho_C\left(\nu_{l,C}+\frac{\nu_{t,C}}{\sigma_\varepsilon}\right)\nabla\varepsilon\right]\\&+\alpha_C\rho_C\frac{\varepsilon}{k}\left(C_{1\varepsilon}P_k-C_{2\varepsilon}\varepsilon\right)+\nabla\cdot\left[\rho_C\frac{\nu_{t,C}}{\sigma_\alpha}\varepsilon\nabla\alpha_C\right]\end{aligned}\tag{13}$$

$$\nu_{t,C}=C_\mu\frac{k^2}{\varepsilon}\tag{14}$$

in which $P_k=2\nu_{t,C}\boldsymbol{D}_C:\nabla\mathbf{U}_C$ is the volumetric production rate of *k* due to the working of the Reynolds stresses against the mean flow. The usual values of the model constants are employed, namely $\sigma_k=1.0$, $\sigma_\varepsilon=1.314$, $C_\mu=0.09$, $C_{1\varepsilon}=1.44$, and $C_{2\varepsilon}=1.92$.

There appears to be no simple model of general validity for evaluation of the particle eddy viscosity $\nu_{t,p}$ in dense particle flows. Nevertheless, even the simple model of $\nu_{t,p}=\nu_{t,C}$ indicated by Issa and Oliveira (1997) was found to yield accurate predictions of the solid volume fraction distribution, which is the focus of this paper.

2.3 Computational domain and boundary conditions

Two validation cases are considered in this work, namely a straight horizontal pipe and a horizontal 90° pipe bend. The two computational domains are reported in Figs. 1 and 2 respectively. In the straight pipe case (Fig. 1), the flow and geometrical symmetry of the phenomenon about the vertical axis (Roco and Shook, 1983; Kaushal et al., 2005) has been exploited by solving only over one half of the pipe section.

In both cases, a fully-developed turbulent flow profile is specified at the pipe inlet, with the distribution of the axial velocity, turbulence kinetic energy and dissipation rate determined from Nikuradse's boundary-layer theory (Schlichting, 1960) for single-phase flow in straight pipes. No slip is assumed between the phases at the inlet section, therefore the same velocity distribution is applied to the fluid and the particles.

$$u_{C,z}^{in}=u_{p,z}^{in}=V_s\frac{(N+1)(2N+1)}{2N^2}\left(1-\frac{2r}{D_p}\right)^{1/N}\qquad N=\frac{1}{\sqrt{f}}$$

$$f=\left[1.82\log(\mathrm{Re})-1.64\right]^{-2}\qquad \mathrm{Re}=\frac{V_s D_p}{\nu_{l,C}}\tag{15}$$

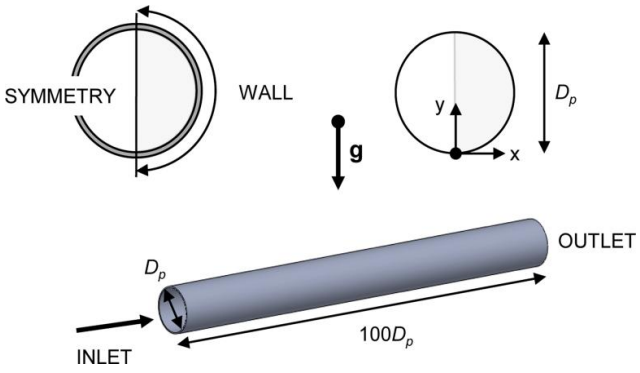

Fig. 1 Computational domain and boundary conditions for horizontal pipe.

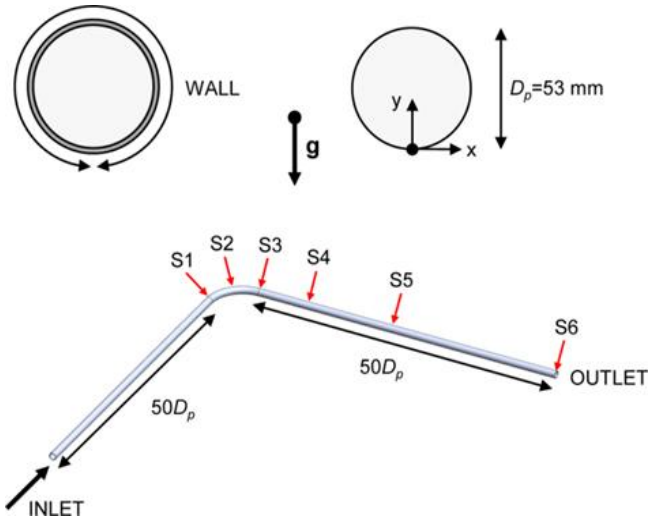

Fig. 2 Computational domain, boundary conditions, and reference sections for 90° bend (S1=bend inlet; S2=bend centre; S3=bend exit; S4=5D_p from bend exit; S5=25D_p from bend exit; S6=50D_p from bend exit).

$$k^{in} = V_s^2 \frac{f}{8}\left[1+\frac{2}{3}\frac{2r}{D_p}+\frac{10}{3}\left(\frac{2r}{D_p}\right)^3\right] \quad (16)$$

$$\varepsilon^{in} = 0.1643\frac{k^{3/2}}{l_m}$$
$$l_m = \frac{D_p}{2}\left[0.14-0.08\frac{2r}{D_p}-0.06\left(\frac{2r}{D_p}\right)^4\right] \quad (17)$$

In Eq. (15), V_s is the superficial velocity of the slurry, which is the ratio between the volumetric slurry flow rate and the pipe area. The inlet volume fractions of both phases are taken as uniformly distributed. At the outlet, the normal gradients of all variables and the value of the pressure are set to zero. The length of the computational domain in the straight pipe case is $100D_p$ to ensure that fully-developed flow conditions are attained, which typically occurs some $50D_p$ downstream of the inlet, confirming the results of previous workers (Ling et al., 2003). For this reason $50D_p$ of straight pipe were simulated upstream the 90° bend (Fig. 2) whilst the outlet boundary is located about $50D_p$ downstream the bend exit in order to analyze the development of the flow downstream the bend and compare the numerical results with the experimental evidence.

At the pipe wall, no slip conditions are imposed to both phases, and the equilibrium wall function of Launder and Spalding (1972) is employed to evaluate the velocity component parallel to the wall for the two phases $u^w_{k=C,p}$, the turbulence kinetic energy k^w, and its dissipation rate ε^w in the near wall cells:

$$\frac{u_k^w}{u_k^*} = \frac{1}{\kappa}\ln\left(E\frac{u_k^* y}{\nu_{l,C}}\right) \quad (18)$$

$$k^w = \frac{u_C^*}{\sqrt{C_\mu}} \quad (19)$$

$$\varepsilon^w = C_\mu^{3/4}\frac{k_w^{3/2}}{\kappa y} \quad (20)$$

where u_k^* is the friction velocity of phase $k = C, p$; $\kappa = 0.41$ is von Karman constant; E is a roughness parameter; and y is the normal distance of the first grid point from the wall. The parameter E is considered as a function of the roughness Reynolds number $\mathrm{Re}_r = u_C^* r_\varepsilon / \nu_{l,C}$, where r_ε is the equivalent sand-grain roughness height. The formula for E, developed by Jayatillika (1969), is as follows.

$$E = \begin{cases} E_m & \mathrm{Re}_r < 3.7 \\ \left[a\left(\frac{\mathrm{Re}_r}{b}\right)^2 + \frac{1-a}{E_m^2}\right]^{-1} & 3.7 < \mathrm{Re}_r < 100 \\ \frac{b}{\mathrm{Re}_r} & \mathrm{Re}_r > 100 \end{cases} \quad (21)$$

where $E_m = 8.6$ is the value of E appropriate for smooth walls, and a and b are given by:

$$a = 1+2x^3-3x^2, \quad x = 0.02248\frac{100-\mathrm{Re}_r}{\mathrm{Re}_r^{0.564}}, \quad b = 29.7 \quad (22)$$

2.4 Computational methodology and consistency of numerical solution

The general-purpose, commercial CFD code PHOENICS was employed for the numerical solution of the finite-volume analogue of the mathematical described above. This was done by using the built-in Eulerian, two-fluid, Inter-Phase Slip Algorithm (IPSA) of Spalding (1980) together with user-defined functions for implementation of specific constitutive equations and boundary conditions. The calculations are performed following the elliptic-staggered formulation in which the scalar variables are evaluated at the cell centers and the velocity components at the cell faces. Central differencing is employed for the diffusion terms, while the convection terms are discretized using the hybrid differencing scheme of Spalding (1972) for the straight pipe case and the MINMOD scheme (Versteeg and Malalasekera, 2007) for the 90° bend. The finite-volume equations are solved iteratively by means of the SIMPLEST and IPSA algorithms of Spalding (1980). The calculation procedure is organized in a slab-by-slab manner, in which all the dependent variables are solved at the current slab before the solver routine moves to the next slab.

The PHOENICS solver was run until the sum of the absolute residual sources over the whole solution domain is less than 1 per cent of reference quantities based on the total inflow of the variable in question. An additional requirement is that the values of the monitored dependent variables at a selected location do not change by more than 0.1% between subsequent iteration cycles.

The consistency of the numerical solution with respect to the domain discretization is now discussed for the two scenarios simulated. A cylindrical-polar structured mesh was employed

in the straight pipe case. A grid sensitivity study was performed to determine the optimum discretization of the domain by reference to the predicted solids volume fraction profiles. For this purpose the following case was taken from Roco and Shook (1983): pipe diameter = 50.7 mm; particle diameter = 520 μm; delivered solid volume fraction = 0.2473; slurry superficial velocity = 2.00 m/s. The pipe is assumed hydraulically smooth ($r_\varepsilon = 0$). This case exhibits a high degree of slurry stratification which is expected to enhance the effect of mesh resolution. Three different meshes were employed, as follows: 9 angular by 12 radial by 85 axial (Grid 1), 12 by 19 by 126 (Grid 2), 15 by 30 by 200 (Grid 3), and 20 by 40 by 300 (Grid 4) cells. For consistency with measurements made using γ-ray density gauges, the predicted solids volume fraction at a distance *y* from the pipe bottom is evaluated by using the chord-average value, i.e:

$$\alpha_p^{\text{chord}}(y) = \frac{1}{x}\int_0^x \alpha_p(x,y)dx \qquad (23)$$

where *x* accounts for the horizontal variation of concentration in the pipe cross-section (Fig. 1). The predicted volume fraction profiles for each grid are shown in Fig. 3. The solutions obtained on the three finest meshes (Grids 2, 3 and 4) are very close to each other, whilst that for Grid 1 deviates slightly from the finer grid solutions. The Grid 3 solution is considered adequate for comparison with the experiments. For each vertical location y, the difference $\left|\alpha_{p,4}^{\text{chord}}(y) - \alpha_{p,3}^{\text{chord}}(y)\right|$ - in which $\alpha_{p,3}^{\text{chord}}$ and $\alpha_{p,4}^{\text{chord}}$ are the values obtained on Grids 3 and 4 respectively - is assumed an indicator of the effect of further mesh refinement. The quantity $\left|\alpha_{p,4}^{\text{chord}}(y) - \alpha_{p,3}^{\text{chord}}(y)\right|$ was found to be lower than 0.005 for all y/D_p, less than the error usually associated with the measurements. The application of the method proposed by Eça and Hoekstra (2006) for estimating the grid discretization error confirmed the reliability of Grid 3.

A curvilinear structured mesh in body-fitted coordinates was instead employed in the 90° bend case. The grid independence study was performed with respect to the following flow condition: particle diameter = 2645 kg/m^3; delivered solid volume fraction = 0.0882; slurry superficial velocity = 2.67 m/s; pipe roughness = 0.015 mm. The four meshes used consisted of: 300 slabwise by 300 axial (Grid 1), 600 by 350 (Grid 2), 1040 by 450 (Grid 3, details of which are shown in Fig. 4), and 1170 by 500 (Grid 4) cells. For consistency

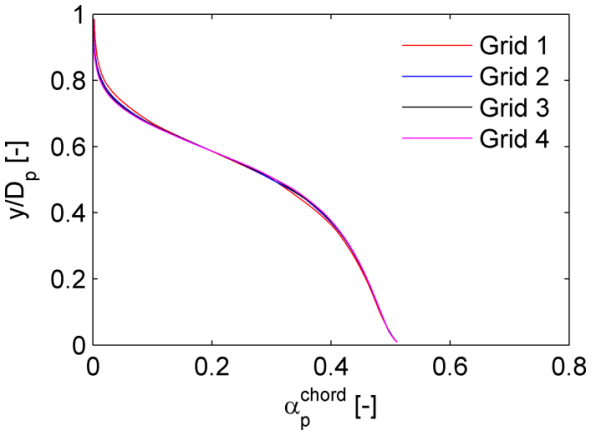

Fig.3 Solid volume fraction profiles calculated on three different grid levels for straight pipe case.

Fig.4 Details of mesh for 90° bend.

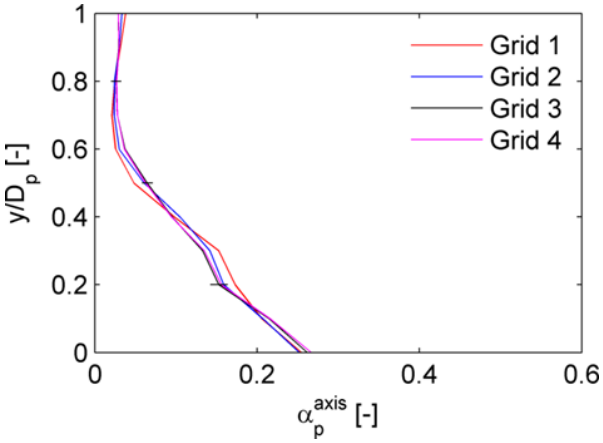

Fig.5 Vertical solid volume fraction profiles at distance of $5D_p$ downstream bend exit (Section S4 in Fig. 2) calculated on different grid levels. The Grid 3 solution has error bars corresponding to the grid discretization error estimated by the method of Eça and Hoekstra (2006).

with the sampling probe measurements of Kaushal et al. (2013), the predicted solids volume fraction at a distance y from the pipe bottom is now evaluated by using the value along the vertical diameter, i.e.:

$$\alpha_p^{axis}(y) = \alpha_p(0, y) \tag{24}$$

The predicted volume fraction profiles for each grid at a distance of $5D_p$ downstream the bend exit (Section S4 in Fig. 2) are shown in Fig. 5, and indicate that Grid 3 is capable to procure a consistent numerical solution, the difference $\left|\alpha_{p,4}^{axis}(y) - \alpha_{p,3}^{axis}(y)\right|$ being less than 0.014 for all y. In Fig. 5, the Grid 3 solution has error bars corresponding to the grid discretization error estimated following the method of Eça and Hoekstra (2006). Grid 3 was used in the simulations.

2.5 Governing terms and calibration of numerical constants

In the two-fluid model different empirical sub-models are employed for the inter-phase processes and closure of the various turbulence correlations. These submodels contain adjustable coefficients which are in practice treated as calibration parameters, their values being determined by matching computations with experiments. The submodels which mainly affect the solid volume fraction distribution refer to two main terms. The former is the phase diffusion of each conserved property ϕ ($\phi = 1$ for mass conservation), equal to $\nabla \cdot (\rho_k D \phi \nabla \alpha_k)$, in which the phase-diffusion coefficient D is given by Eq. (2). The phase diffusion, besides making the model numerically more stable and thereby contributing to its speed in attaining convergence, has a smoothing effect on the solids concentration profile, reducing its variation along the vertical direction. The impact of phase diffusion is controlled by an empirical parameter, which is the turbulent Schmidt number for volume fractions σ_α which appear in Eq. (2). A sensitivity analysis to quantify the influence of σ_α on the solid volume fraction profile was performed.

The results are depicted in Fig. 6 for horizontal pipe flows with very different flow conditions, both taken from Roco and Shook (1983): A) pipe diameter = 51.5 mm; particle diameter = 165 μm; particle density = 2650 kg/m^3; delivered solid volume fraction = 0.09; slurry superficial velocity = 3.78 m/s; B) pipe diameter = 50.7 mm; particle diameter = 520 μm; particle density = 2650 kg/m^3; delivered solid volume fraction = 0.2473; slurry superficial velocity = 2.00 m/s. In both cases, the pipe is regarded is hydraulically smooth. It is observed that a reduction of σ_α results in a flatter profile as a consequence of the increase in diffusivity.

The latter term which most influences the solid volume fraction profile is the interfacial momentum transfer (Eq. (6)) and, particularly, the drag force (Eq. (7)). As already noticed, the definition of the particle Reynolds number with respect to the viscosity of the mixture μ_m, instead of that of the fluid phase μ_C, puts an upper limit to the solids concentration due to the asymptotic trend of μ_m (Eq. (11)). The mixture viscosity, as derived from the correlation of Mooney (Eq. (11)), depends on two empirical parameters, the intrinsic viscosity $[\eta]$ and the maximum packing concentration α_{pm}. The effect of $[\eta]$ and α_{pm} on

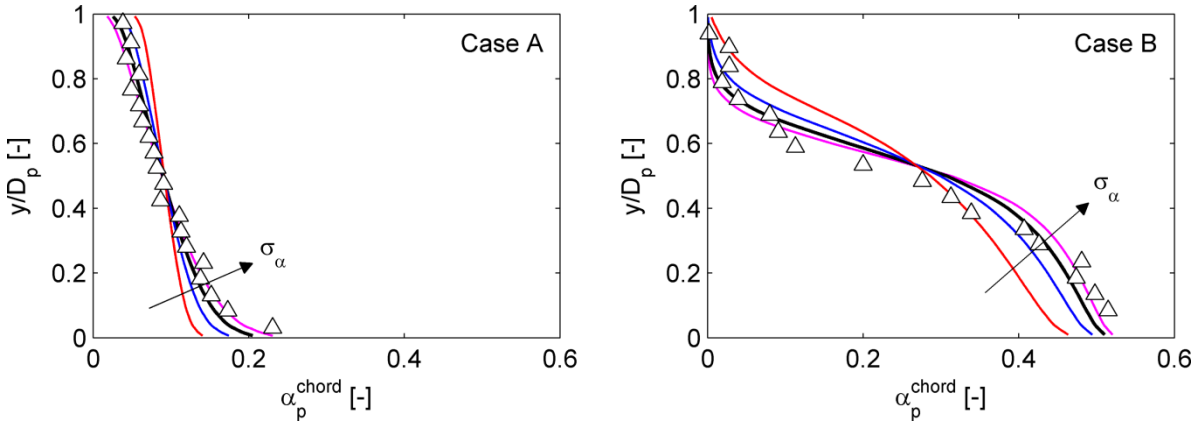

Fig. 6 Effect of turbulent Schmidt number for volume fractions σ_α on solid volume fraction profiles for two flow conditions (△: experiments from Roco and Shook (1983); ——: $\sigma_\alpha = 0.3$; ——: $\sigma_\alpha = 0.5$; ——: $\sigma_\alpha = 0.7$; ——: $\sigma_\alpha = 0.9$).

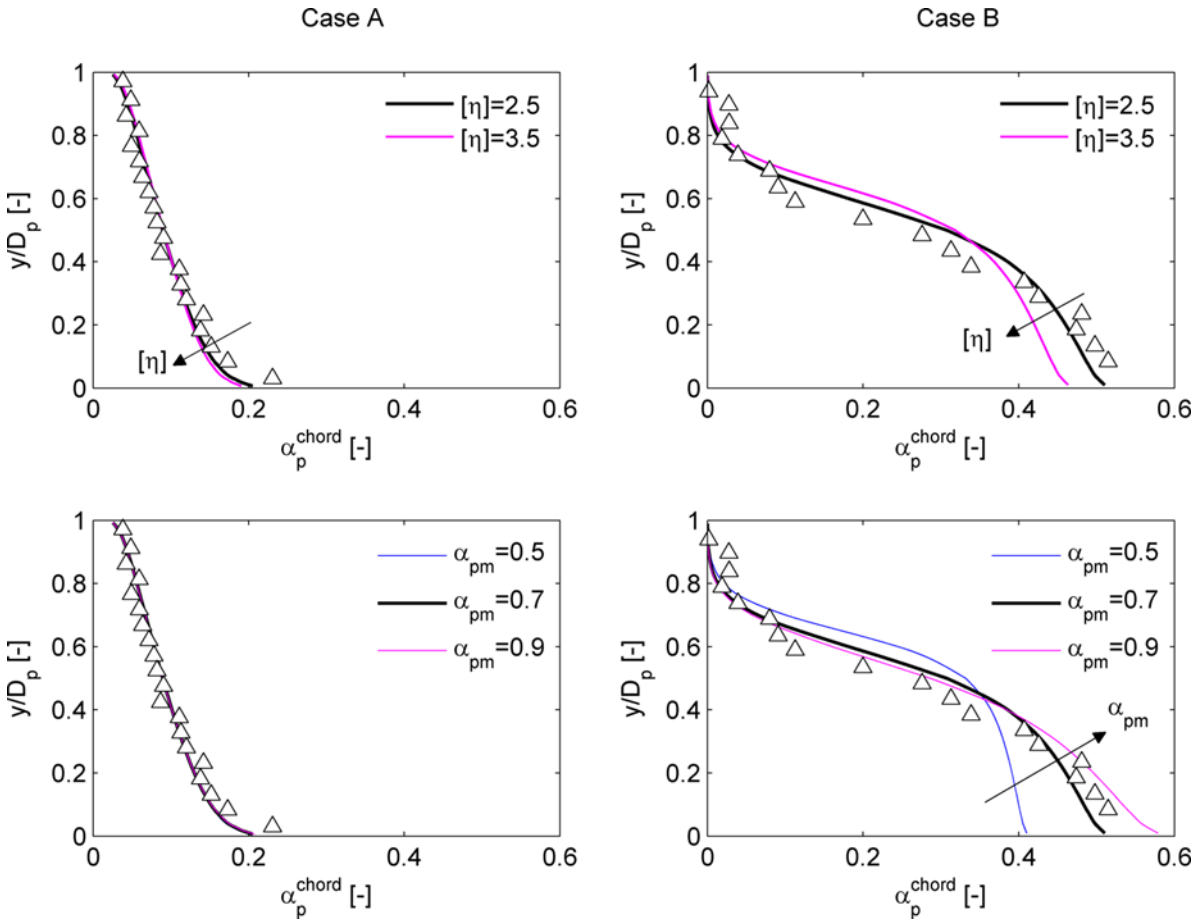

Fig. 7 Effect of parameters [η] and α_{pm} in mixture viscosity correlation of Mooney (Eq. 11) on solid volume fraction profiles for two flow conditions (△: experiments from Roco and Shook (1983); continuous lines: predictions). The dependence on [η] is studied for $\alpha_{pm} = 0.7$; that on α_{pm} for [η] = 2.5.

Table 1 Flow conditions considered for comparison.

Reference	System	D_p [mm]	r_ε / D_p [-]	d_p [μm]	C [%]	V_s [m/s]	ρ_p [kg/m^3]
Roco and Shook (1983)	Pipe	50.7-51.5	-	165-520	9.0-29.6	1.90-4.33	2650
Gillies et al. (2004)	Pipe	103.0	$2\cdot10^{-5}$	90-280	10.6-40.7	1.33-5.40	2650
Matousek (2000 and 2002)	Pipe	150.0	-	120-370	25.0-43.0	2.04-6.00	-
Shaan et al. (2000)	Pipe	158.5	$6\cdot10^{-6}$	90	15.0-32.0	1.40-3.00	2655
Kaushal et al. (2013)	90° Bend	53.0	$3\cdot10^{-4}$	450	8.82	2.67	2645

the solid volume fraction profile is analyzed one at a time in Fig. 7 for the two above mentioned flow conditions from Roco and Shook (1983). In particular, the results highlight that α_{pm} affects the behaviour of the mixture only at high concentration, therefore as a direct effect on the prevention of particle over-packing. As already mentioned, this avoids the need to introduce a collisional pressure term in the momentum equation of the solid phase, further promoting the numerical stability of the model and the rapid achievement of a converged solution.

Our investigations showed that a unique combination of the three empirical parameters – $\sigma_\alpha = 0.7$, $[\eta] = 2.5$ and $\alpha_{pm} = 0.7$ (all within the range of variability found in literature) – produced estimations of the solids concentration profile in good agreement with the experimental evidence for all the flow conditions considered in the present work, referring to both the horizontal pipe case and the 90° bend case. This feature, together with the numerical stability and the relatively short computer time required, contributes to make the model particularly useful for the applications.

3. RESULTS

The numerical model is validated by comparing the results of the simulations against experimental data reported by the authors listed in Table 1. This

table provides the flow conditions for each set of measurements. As already mentioned, two scenarios have been considered, namely a straight horizontal pipe and a 90° bend, which will be discussed in separate sub-sections.

3.1 Straight horizontal pipe

The predictions of the model have been compared with experimental data for 26 flow conditions, summarized in Table 2, which differ in terms of pipe diameter, pipe roughness, particle size, slurry superficial velocity, and delivered solid volume fraction. Each set of measurements allows an assessment of the model's capability for reproducing the influence of specific features affecting the distribution of the solid volume fraction. The data of Roco and Shook (1983) and Gillies et al. (2004) are used to investigate the effect of particle diameter and slurry velocity with different delivered solid volume fraction. The measurements of Matousek (2000, 2002) provide the opportunity to extend the validity of the model up to a pipe Reynolds number Re (Eq. (15)) of about 10^6. Finally, the data of Shaan et al. (2000) are used to assess the performance of the model in case of natural sands with irregularly-shaped grains. Almost all the data refer to configurations in which all the solids are kept suspended, but moving bed flows have also been briefly explored to check how far one can go in employing the model for the purpose of achieving useful information from an engineering point of view.

Measurements of solids concentration – either bulk-mean or local – are subjected to errors depending mainly on the instrumentation used, as discussed in Section 1. All the data reported in Table 2 are obtained using gamma-ray absorption methods, perhaps the technique which provides the highest accuracy attainable, with errors of the order of a few percentage points. Since this technique allows measuring chord-average values of solid volume fraction, the computed volume fraction profile was evaluated by means of Eq. (23). In the experiments from Roco and Shook (1983) – cases A1 to A5 in Table 2 – the dispersed phase consists of three kinds of sand, with narrow size distribution and mean particle diameters of 165 and 520 μm. The solids density is 2650 kg/m^3, the pipe diameter is about 51 mm,

Table 2 Details of experimental conditions for straight pipe case (A1 to A5: experimental data from Roco and Shook (1983); B1 to B12: experimental data from Gillies et al. (2004); C1 to C6: experimental data from Matousek (2000 and 2002); D1 to D4: experimental data from Shaan et al. (2000); * values not declared by experimenters).

Test ID	D_p [mm]	r_ε / D_p [-]	d_p [μm]	C [%]	V_s [m/s]	ρ_p [kg/m^3]	Flow pattern
A1	51.5	0*	165	9	3.78	2650	FS
A2	51.5	0*	165	19	4.17	2650	FS
A3	51.5	0*	165	28	4.33	2650	FS
A4	50.7	0*	520	12.12	1.90	2650	MB
A5	50.7	0*	520	24.73	2.00	2650	MB
B1	103	$2\cdot10^{-5}$	90	19.8	1.33	2650	FS
B2	103	$2\cdot10^{-5}$	90	28.3	1.33	2650	FS
B3	103	$2\cdot10^{-5}$	90	19	3.00	2650	FS
B4	103	$2\cdot10^{-5}$	90	28.4	3.00	2650	FS
B5	103	$2\cdot10^{-5}$	280	12	2.55	2650	FS
B6	103	$2\cdot10^{-5}$	280	20.8	2.60	2650	FS
B7	103	$2\cdot10^{-5}$	280	31.0	2.50	2650	FS
B8	103	$2\cdot10^{-5}$	280	40.7	2.60	2650	FS
B9	103	$2\cdot10^{-5}$	280	10.6	5.40	2650	FS
B10	103	$2\cdot10^{-5}$	280	20.3	5.40	2650	FS
B11	103	$2\cdot10^{-5}$	280	30.1	5.40	2650	FS
B12	103	$2\cdot10^{-5}$	280	40.5	5.40	2650	FS
C1	150	0*	120	25	2.04	2650*	FS
C2	150	0*	120	35	2.04	2650*	-
C3	150	0*	120	34	6.00	2650*	-
C4	150	0*	370	25	6.00	2650*	FS
C5	150	0*	370	34	6.00	2650*	-
C6	150	0*	370	43	6.00	2650*	MB
D1	158.5	$6\cdot10^{-6}$	90	15	1.5	2655	FS
D2	158.5	$6\cdot10^{-6}$	90	32	1.4	2655	FS
D3	158.5	$6\cdot10^{-6}$	90	15	3.0	2655	FS
D4	158.5	$6\cdot10^{-6}$	90	32	3.0	2655	FS

the slurry bulk-mean velocity varies from 1.90 to 4.33 m/s, and the pipe Reynolds number from between $9.6 \cdot 10^4$ and $2.1 \cdot 10^5$. The delivered solid volume fraction ranges from 9% to 30%. The authors did not indicate the roughness of the pipe, which was assumed hydraulically smooth. No evaluation of measurement uncertainty was reported by the experimenters, and they did not identify the flow patterns according to the more recent classification of Doron and Barnea (1996). However, for the smallest particle diameter the data suggest suspended flow, whereas for the largest diameter the indications are for moving-bed flow. Fig. 8 compares the computed and measured solid volume fraction profiles. The good agreement between computation and measurements reveals the ability of the model to reproduce the effect of particle diameter on the particle distribution for slurries with different delivered solid volume fraction. The simple two-fluid model proposed in this work appears capable to predict with reasonable accuracy the solid volume fraction profile not only in case of fully-suspended flow, but also in case of moving bed flows. This indicates that the asymptotic trend of the interfacial momentum transfer term

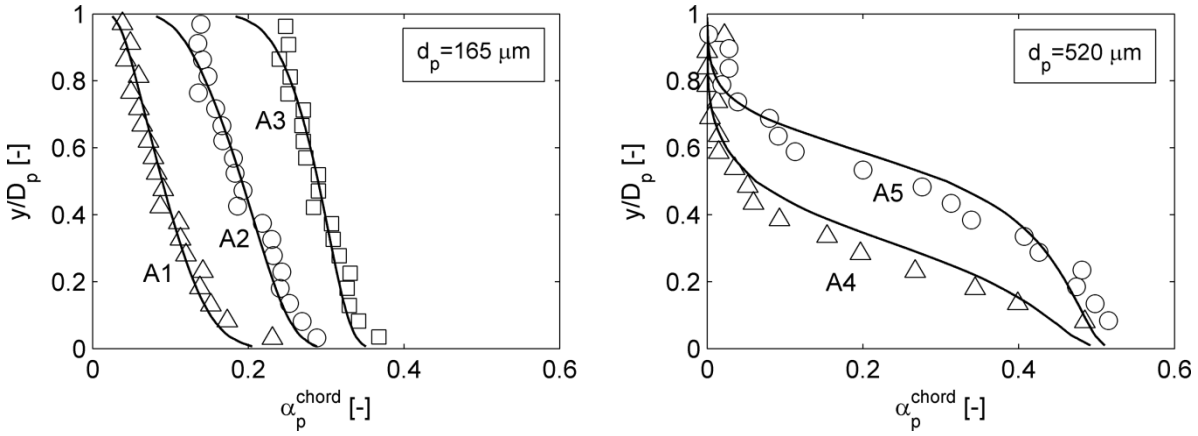

Fig. 8 Solids concentration profiles for flow conditions A1 to A5 in Table 2 (△○□: experiments from Roco and Shook (1983); ——: predictions).

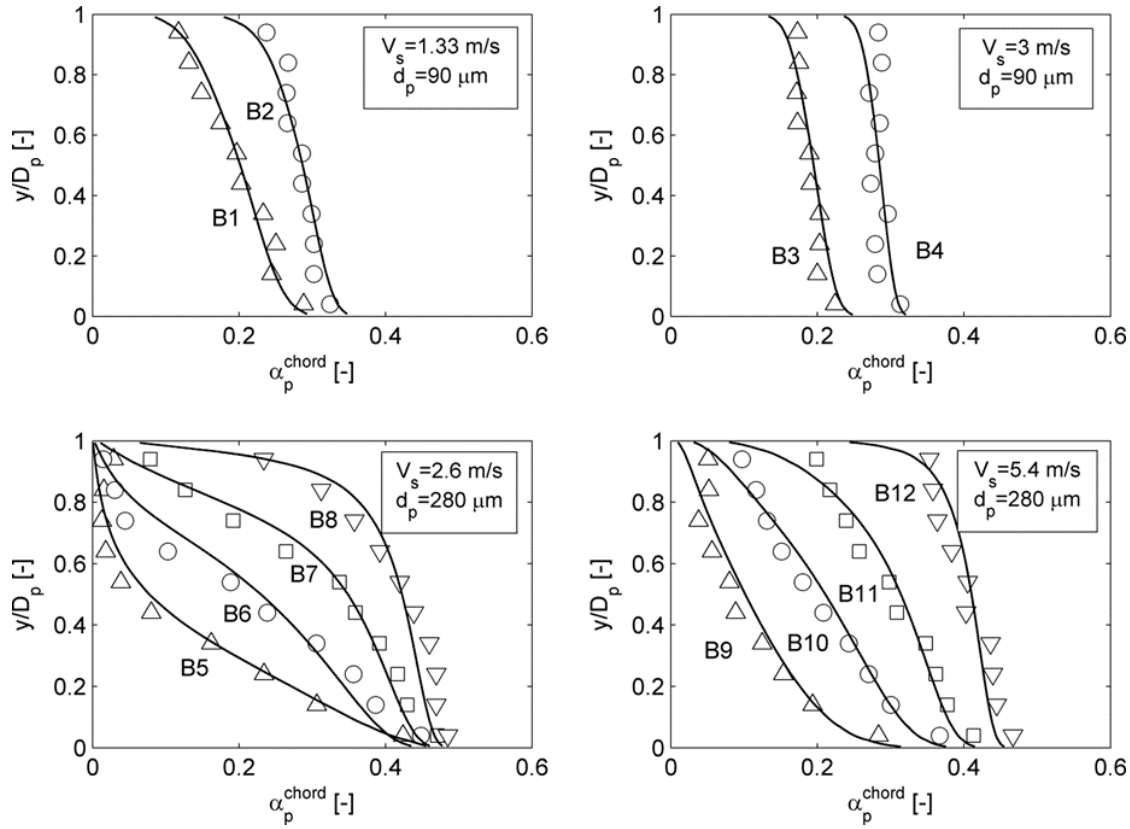

Fig. 9 Solids concentration profile for flow conditions B1 to B12 in Table 2 (△○□▽: experiments from Gillies et al. (2004); ——: predictions).

produces on the solid volume fraction profile the same effect that is traditionally achieved by the collisional pressure and the tensor $\boldsymbol{T}_{v,k}$.

Gillies et al. (2004) measured the concentration profiles of sand-water slurries in a 103 mm diameter pipe using gamma-ray absorption gauges, without reporting the uncertainty. The roughness of the pipe is 2 nm. Two kinds of sand were considered, with narrow size distribution and mean particle diameter of 90 and 280 μm. In both cases the particle density was 2650 kg/m^3, and the slurry superficial velocity varies from 1.33 to 5.4 m/s (corresponding to a pipe Reynolds number between $1.4 \cdot 10^5$ and $5.6 \cdot 10^5$). The delivered solid volume fraction varies from about 10% to about 45%. Details of the flow conditions considered for comparison are reported in Table 2, cases B1 to B12. From an examination of the measured data for the pressure gradient, it can be inferred that in all cases the flow is fully-suspended. This is a good test for the model's ability to predict the combined effect of slurry velocity, solids loading, and particle diameter in a larger pipe. Fig. 9 shows comparison of the computational and the experimental results for the vertical distribution of the solid volume fraction. The model produces good overall agreement with the data. The largest deviations are observed near the pipe wall for the small particles at high concentration (cases B2 and B4 in Table 4), but as noted by the authors themselves these measurements are subject to the largest experimental error.

Matousek (2000 and 2002) measured the concentration profiles of sand-water slurries in a 150 mm diameter pipe using gamma-ray absorption method, quantifying a 4% uncertainty of the data. We reproduced numerically the flow conditions reported in Table 2 (cases C1 to C6), in which the dispersed phase consists of two kinds of sand with narrow size distribution and mean particle diameters of 120 and 370 μm. Unfortunately neither the density of the solid particles nor the pipe roughness are reported in the experiments of Matousek (2000 and 2002); and so in the simulations the former was set to 2650 kg/m^3, which is the value declared by Roco and Shook (1983) and Gillies et al. (2004), and the pipe was regarded as hydraulically smooth. The slurry superficial velocity was 2 or 6 m/s, corresponding to a pipe Reynolds number up to 10^6. The delivered solid volume fraction ranged between 25 and 43%. According to the author, the flows are either fully suspended or with a moving bed, but only for three cases the flow pattern could be clearly identified from the plot of pressure gradient versus slurry superficial velocity. Fig. 10 compares the computed and measured solid volume fraction profiles; each set of experimental data has error bars indicating the uncertainty declared by the experimenter. The rather good agreement between computations and measurements confirm the reliability of the model for high pipe Reynolds numbers. A closer inspection reveals that for case C6 the computed concentration is lower than the experimental results in the lower part of the pipe and higher in the upper region. However, the pressure gradient curve clearly reveals that in case C6 a moving bed of particles is formed. It is again confirmed that the proposed model is capable to procure a rough indication of the distribution of the solid also for flows in which the inter-granular stresses play an important role.

Moreover, in the case of highly dense slurries like case C6, the experimental data are subject to the most uncertainty, and the numerical solutions are sensitive to the empirical parameters α_{pm} and $[\eta]$ which appear in the mixture viscosity correlation (Eq. (11)). For the same case, the measured solids concentration profile shows a drop near the pipe bottom. This reversal is not predicted by the numerical model, which is probably due to the absence of the wall lift force discussed earlier in Section 2.1. The same limitation was reported by Ekambara et al. (2009).

The paper of Shaan et al. (2000) focuses on the effect of particle shape upon pressure gradient and deposition velocity, but these workers also reported some measurements of the solid volume fraction profiles. Shaan et al. (2000) quantified the particle shape by reference to the following quantities, evaluated from photos of the particles: the axes ratio, i.e. the ratio between the major and minor axes of an ellipse circumscribing the grains; the circularity index, i.e. the ratio between the area of the particle, multiplied by 4π, and its perimeter. The sand particles have a very irregular shape, as can be inferred by comparing the measured values of axes ratio (1.6) and circularity (0.62) against typical values reported in the literature for sand grains. The mass-median value of the particle size distribution curve is taken as the characteristic particle diameter. The flow conditions reported in Table 2 (cases D1 to D4) were reproduced to check the behaviour of the model for the case of irregularly-shaped sand particles. The pipe diameter (158.5 mm), delivered solid volume fraction (15% or 35%), slurry superficial velocity (1.4 or 3 m/s), particle density (2655 Kg/m^3), and particle diameter (90 μm) are all approximately within the range

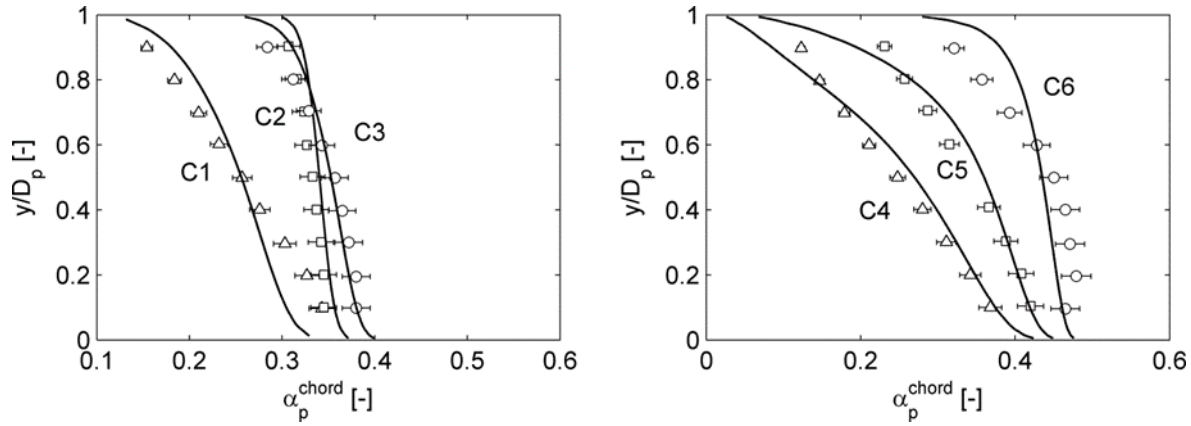

Fig. 10 Solids concentration profiles for flow conditions C1 to C6 in Table 2 (△○□: experiments from Matousek (2000 and 2002); ——: predictions).

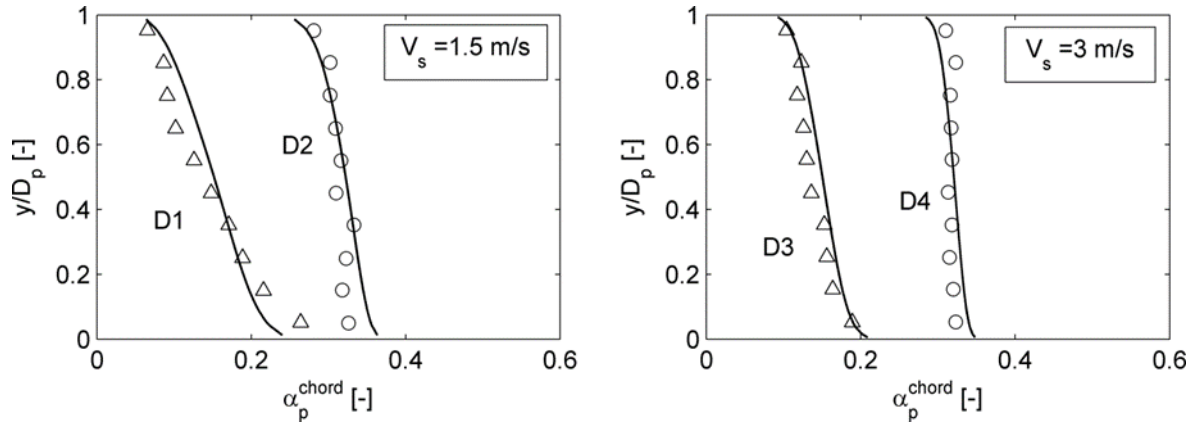

Fig. 11 Solids concentration profiles for flow conditions D1 to D4 in Table 2 (△○: experiments from Shaan et al. (2000); ——: predictions).

covered by the earlier simulations.

The numerical and experimental results are compared in Fig. 11. The agreement between the numerical predictions and the experimental evidence is fairly good; inadequacies of the numerical model – especially in the wall boundary conditions for the solid phase – and measurements error can both contribute to the discrepancies observed near the pipe bottom for case D2. The results seem to indicate that the numerical model is a suitable tool for predicting the solid volume fraction distribution produced by sands with a very irregular shape.

3.2 Horizontal 90° bend

The predictions of the model have been compared with the recent experiments of Kaushal et al. (2013) regarding a horizontal 90° bend. Among the different flow conditions considered by these authors, reference is made to those characterized by delivered solid volume fraction of 8.82%, within the range of interest in this work. The experimenters used a sampling probe to measure the volume fraction profile of the slurry in the 53 mm diameter pipe along the vertical axis at distances of $5D_p$, $25D_p$, and $50D_p$ downstream the bend exit (referred to as sections S4, S5, and S6 in Fig. 2, respectively). They quantified a 2% uncertainty of the data. The solid phase consists of silica sand particles with narrow size distribution and mean particle diameter of 450 μm. The slurry superficial velocity is 1.78, 2.67, or 3.56 m/s.

The flow within the bend is much more complex compared to that through the straight pipe since secondary motions develop in the crosswise direction. These motions affect significantly the distribution of the solids and, as a consequence, the volume fraction distribution is no longer constant over horizontal planes. This is evident in Fig. 12, which shows the color plot of the solids volumetric concentration over the six cross sections highlighted in Fig. 2. As shown in Fig. 13, the predictions of our model generally agree with the experimental data available. Greater discrepancies are observed for the highest superficial velocity (3.56 m/s), where the model seems to underestimate the quantity of particles dragged by the secondary motions. This is

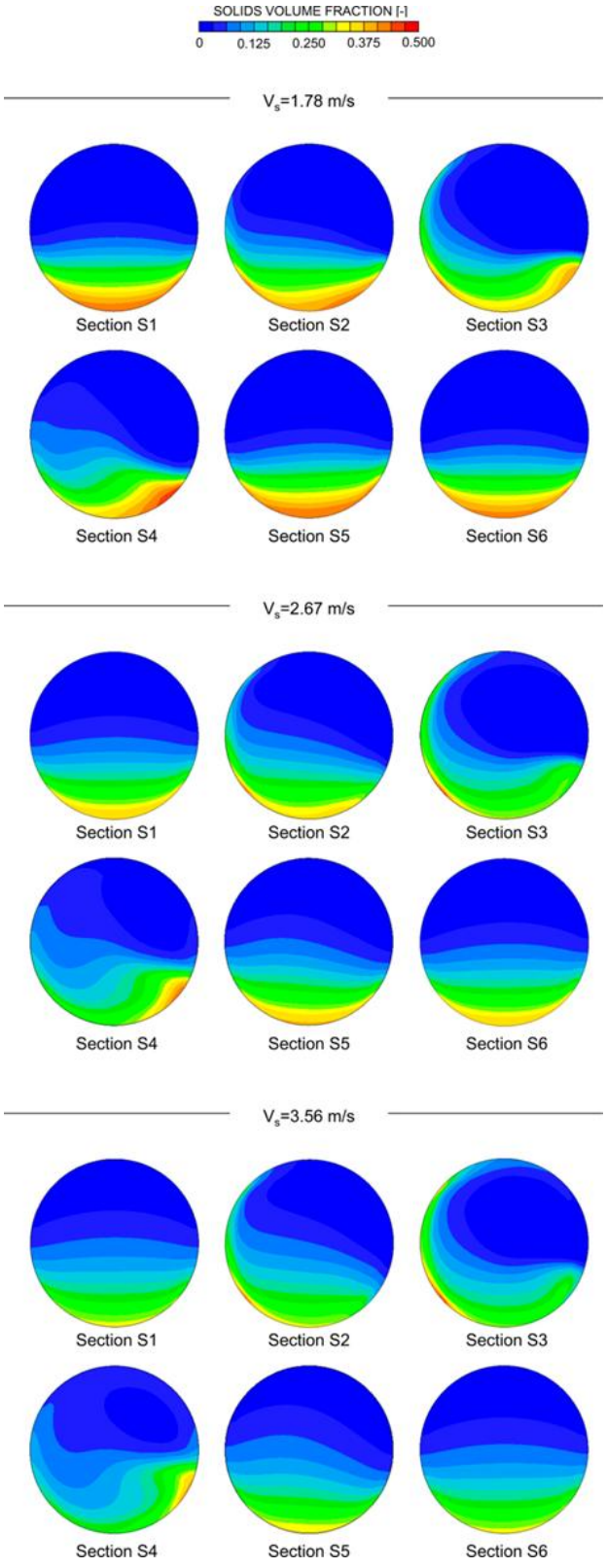

Fig. 12 Solid volume fraction distributions on sections S1 to S6 in Fig. 2 for delivered solid volume fraction of 8.82%. Left hand side is the outer wall of the pipe.

opposite to the KTGF based model of Kaushal et al. (2013), which tends to over-enhance the effect of the secondary motions on the solids for the lowest velocities. Fig. 13 also reveals that our model tends to overestimate the solids volume fraction close to the pipe bottom far from the bend exit. It is expected that the predictions could be improved if the effect of the wall lubrication force, for which a suitable model does not exist at present, were accounted for.

4. CONCLUSIONS

A mathematical model has been described for the estimation of solid volume fraction distribution of solid-liquid slurry flows in horizontal pipes and bends. The model is based on an Eulerian-Eulerian approach, and uses the Inter-Phase Slip Algorithm (IPSA) of Spalding (1980). The novelty of this model resides in the combined use of existing modelling strategies never previously employed simultaneously for the predictions of slurry flows. In order to account for turbulent dispersion of particles, phase diffusion terms have been included in the phase continuity equations, together with all the conservation equations. The mixture viscosity approach is adopted to model the effect of multiple particles on the inter-phase friction. A wall function is employed to model the flow in the near-wall region in case of both hydraulically smooth and rough walls. All these strategies result in a model which, despite being simpler that those commonly used for addressing solid-liquid slurry flows, shows comparable or even better predictive capacity. Moreover, this model is robust and numerically stable, and requires relatively short CPU time to procure converged steady-state solutions.

The model has been first validated by comparison with experimental data for the horizontal pipe case over a wide range of operating conditions: delivered solid volume fraction between 10% and 40% by volume; mean particle diameter between 90 and 520 μm; slurry superficial velocity between 1 m/s and 5.5 m/s; and pipe diameter between 50 and 158 mm. The model predictions were found to be in good agreement with the experimental evidence for all the flow conditions considered for comparison. Even if the model is originally intended to address fully-suspended flows, the results indicated its capability to provide rough indications of the solid volume fraction distribution also in case of bed flows.

At last, the comparison with the recent measurements of Kaushal et al. (2013) revealed that this model is capable to procure reliable predictions of the particle distribution downstream a 90° bend in a horizontal pipe.

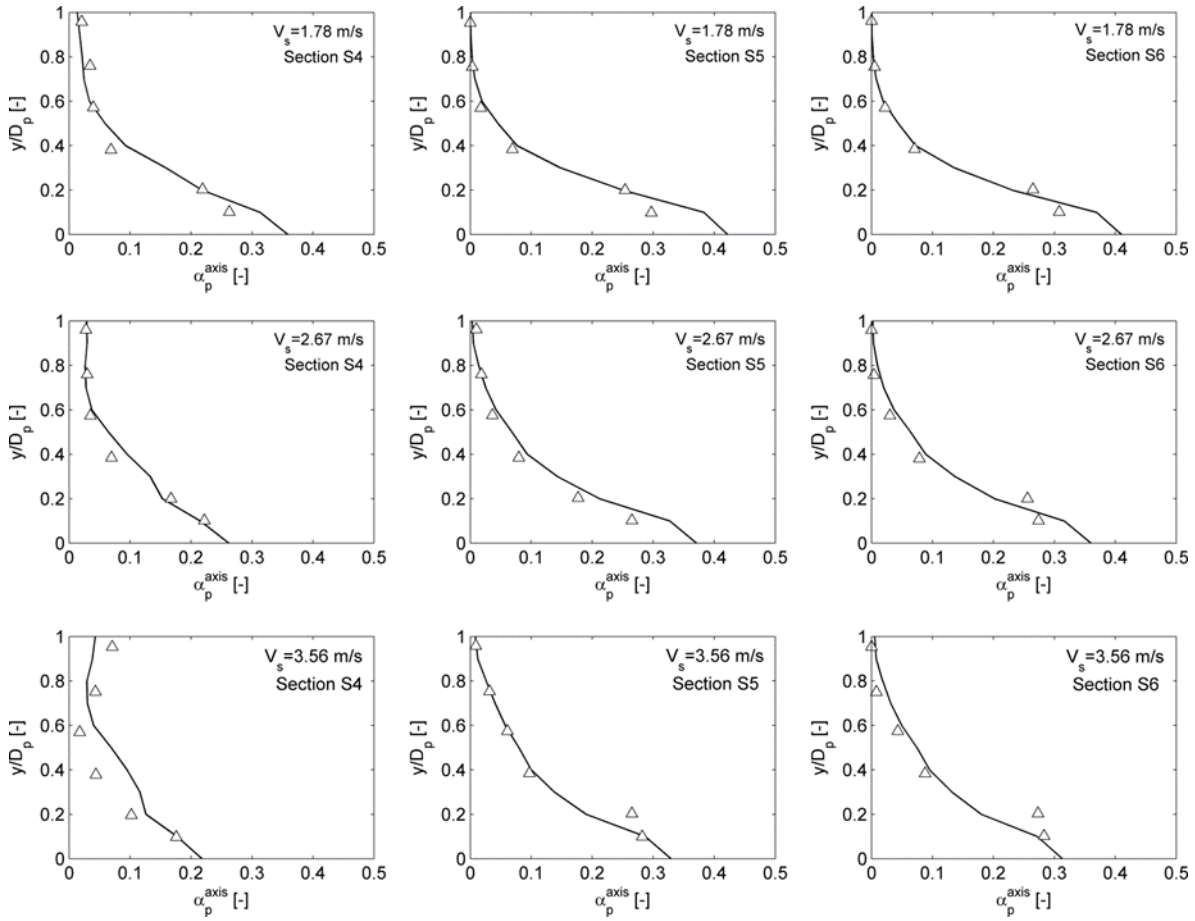

Fig. 13 Solid volume fraction along vertical diameter on sections S4 to S6 in Fig. 2 for delivered solid volume fraction of 8.82% (△: experiments from Kaushal et al. (2013); ——: predictions).

ACKNOWLEDGEMENTS

The authors would acknowledge the CINECA and the Regione Lombardia award under the LISA initiative, for the availability of high performance computing resources and support. The authors would like to thank CHAM Ltd for supporting this research and acknowledge Dr. Randy Gillies of Saskatchewan Research Council for providing his experimental data.

REFERENCES

1. Ahilan RV, Sleath J (1987). Sediment transport in oscillatory flow over flat beds. *Journal of Hydraulic Engineering* 113: 308-322.
2. Albunaga BE (2002). *Slurry Systems Handbook* McGraw-Hill.
3. Antal S, Lahey R, Flaherty J (1991). Analysis of phase distribution in fully-developed laminar bubbly two phase flow. *International Journal of Multiphase Flow* 17(5): 635-652.
4. Barnea E, Mizrahi J (1973). A Generalized Approach to the Fluid Dynamics of Particulate Systems. *Chemical Engineering Science* 5(2): 171-189.
5. Chen L, Duan Y, Pu W, Zhao C (2009). CFD simulation of coal-water slurry flowing in horizontal pipelines. *Korean Journal of Chemical Engineering* 26(4): 1144-1154.
6. Chen RC (1994). Analysis of homogeneous slurry pipe flow. *Journal of Marine Science and Technology* 2(1): 37-45.
7. Chen X, Li Y, Niu X, Li M, Chen D, Yu X (2011). A general two-phase turbulent flow model applied to the study of sediment transport in open channels. *International Journal of Multiphase Flow* 37(9): 1099-1108.
8. Chung JN, Troutt TR (1988). Simulation of particle dispersion in an axisymmetric jet. *Journal of Fluid Mechanics* 186: 199-222.
9. Clift R, Grace JR, Weber ME (1978). *Bubbles, Drops and Particles*. Academic Press.
10. Colwell JM, Shook CA (1988). The Entry Length for Slurries in Horizontal Pipeline Flow. *Canadian Journal of Chemical Engineering* 66(5): 714-720.

11. Doron P, Barnea D (1993). A three layer model for solid-liquid flow in horizontal pipes. *International Journal of Multiphase Flow* 19(6): 1029-1043.
12. Doron P, Barnea D (1995). Pressure drop and limit deposit velocity for solid-liquid flow in pipes. *Chemical Engineering and Science* 50(10): 1595-1604.
13. Doron P, Barnea D (1996). Flow pattern maps for solid-liquid flow in pipes. *International Journal of Multiphase Flow* 22(2): 273-283.
14. Doron P, Granica D, Barnea D (1987). Slurry flow in horizontal pipes – experimental and modeling. *International Journal of Multiphase Flow* 13(4): 535–547**.**
15. Eça L, Hoekstra M (2006). Discretization uncertainty estimation based on a least squares version of the grid convergence index. *Proceedings of the 2nd Workshop on CFD Uncertainty Analysis,* Oct 19-20, Lisbon, Portugal.
16. Ekambara K, Sanders RS, Nandakumar K, Masliyah JH (2009). Hydrodynamic simulation of horizontal slurry pipeline flow using ANSYS-CFX. *Industrial & Engineering Chemistry Research* 48(17): 8159-8171.
17. Gillies RG, Shook CA (2000). Modelling High Concentration Settling Slurry Flows. *Canadian Journal of Chemical Engineering* 78(4): 709-716.
18. Gillies RG, Shook CA, Xu J (2004). Modelling Heterogeneous Slurry Flow at High Velocities. *Canadian Journal of Chemical Engineering* 82(5): 1060-1065.
19. Hsu, FLG (1981). *Flow of Fine-particle Suspensions in Bends, Fittings and Valves*. MS Thesis, Texas Tech. University, Lubbock, Texas, USA.
20. Ishii M, Mishima K (1984). Two-fluid model and hydrodynamic constitutive relations. *Nuclear Engineering and Design* 82(2-3): 107-126.
21. Issa RI, Oliveira PJ (1997). Assessment of a particle-turbulence interaction model in conjunction with an Eulerian two-phase flow formulation. *Proceedings of the 2nd International Symposium on Turbulence, Heat and Mass Transfer,* June 9-12, Delft, Netherlands, 759-770.
22. Jayatillika CLV (1969). The influence of the Prandtl number and surface roughness on the resistance of the sublayer to momentum and heat transfer. *Progress in Heat & Mass Transfer* 1: 193-329.
23. Jiang YY, Zhang P (2012). Pressure drop and flow pattern of slush nitrogen in a horizontal pipe. *AIChE Journal* doi: 10.002/aic.13927.
24. Kaushal DR, Kumar A, Tomita Y, Juchii S, Tsukamoto H (2013). Flow of mono-dispersed particles through horizontal bend. *International Journal of Multiphase Flow* 52: 71-91.
25. Kaushal DR, Sato K, Toyota T, Funatsu K, Tomita Y (2005). Effect of particle size distribution on pressure drop and concentration profile in pipeline flow of highly concentrated slurry. *International Journal of Multiphase Flow* 31(7): 809-823.
26. Kaushal DR, Thinglas T, Tomita Y, Juchii S, Tsukamoto H (2012). CFD modeling for pipeline flow of fine particles at high concentration. *International Journal of Multiphase Flow* 43: 85-100.
27. Kaushal DR, Tomita Y (2003). Comparative study of pressure drop in multisized particulate slurry flow through pipe and rectangular duct. *International Journal of Multiphase Flow* 29(9): 1473-1487.
28. Kaushal DR, Tomita Y (2007). Experimental investigation for near-wall lift of coarser particles in slurry pipeline using γ-ray densitometer. *Powder Technology* 172(3): 177-187.
29. Kim C, Lee M, Han C (2008). Hydraulic transport of sand-water mixtures in pipelines. Part I. Experiment. *Journal of Mechanical Science and Technology* 22(12): 2534-2541.
30. Kumar U, Mishra R, Singh SN, Seshadri V (2003). Effect of particle gradation on flow characteristics of ash disposal pipelines. *Powder Technology* 132(1): 39-51.
31. Lahiri SK, Ghanta KC (2010). Slurry flow modeling by CFD. *Chemical Industry & Chemical Engineering Quarterly* 16(4): 295-308.
32. Launder BE, Spalding DB (1972). *Mathematical models of turbulence*. Academic Press.
33. Ling J, Skudarnov PV, Lin CX, Ebadian MA (2003). Numerical investigations of solid-liquid slurry flows in a fully developed flow region. *International Journal of Heat and Fluid Flow* 24(3): 389-398.
34. Matousek V (2000). Concentration distribution in pipeline flow of sand-water mixtures. *Journal of Hydrology and Hydromechanics* 48(3): 180-196.
35. Matousek V (2002). Pressure drops and flow patterns in sand-mixture pipes. *Experimental*

Thermal and Fluid Science 26(6-7): 693-702.
36. Matousek V (2009). Predictive model for frictional pressure drop in settling-slurry pipe with stationary deposit. *Powder Technology* 192(3): 367-374.
37. Mooney M (1951). The viscosity of a concentrated suspension of spherical particles. *Journal of Colloid Science* 6(2): 162-170.
38. Nasr-el-Din H, Shook CA, Esmail MN (1984). Isokinetic Probe Sampling From Slurry Pipelines. *Canadian Journal of Chemical Engineering* 62(2): 179-185.
39. Pathak M (2011). Computational investigations of solid-liquid particle interaction in a two-phase flow around a ducted obstruction. *Journal of Hydraulic Research* 49(1), 96-104.
40. Pecker SM, Helvaci SS (2008). *Solid-Liquid Two-Phase Flow*. Elsevier.
41. Roco MC, Shook CA (1983). Modeling of Slurry Flow: The Effect of Particle Size. *Canadian Journal of Chemical Engineering* 61(4): 494-503.
42. Schlichting H (1960). *Boundary Layer Theory*. McGraw-Hill.
43. Shaan J, Sumner RJ, Gillies RG, Shook CA (2000). The Effect of Particle Shape on Pipeline Friction for Newtonian Slurries of Fine Particles. *Canadian Journal of Chemical Engineering* 78(4): 717-725.
44. Shiller L, Naumann A. (1935). A drag coefficient correlation. *Zeitschrift des Vereines Deutscher Ingenieure* 77: 318-320.
45. Shirolkar JS, Coimbra CFM, McQuay MQ (1996). Fundamental aspects of modelling turbulent particle dispersion in dilute flows. *Progress in Energy and Combustion Science* 22(4): 363-399.
46. Shook CA, Bartosik AS (1994). Particle-wall stresses in vertical slurry flows. *Powder Technology* 81(2): 117-124.
47. Skudarnov PV, Lin CX, Ebadian MA (2004). Double-Species Slurry Flow in a Horizontal Pipeline. *ASME Journal of Fluids Engineering* 126(1): 125-132.
48. Spalding DB (1972). A novel finite-difference formulation for differential expressions involving both first and second derivatives. *International Journal of Numerical Methods in Engineering* 4(4): 551-559.
49. Spalding DB (1980). Numerical computation of multi-phase fluid flow and heat transfer. In: Taylor C, Morgan K (Eds.), *Recent Advances in Numerical Methods in Fluids*, Pineridge Press Limited, 139-168.
50. Turian RM, Ma TW, Hsu FLG, Sung MDJ, Plackmann GW (1998). Flow of concentrated non-Newtonian slurries: 2. Friction losses in bends, fittings, valves, and Venturi meters. *International Journal of Multiphase Flow* 24(2): 243-269.
51. Versteeg HK, Malalasekera W (2007). *An Introduction to Computational Fluid Dynamics. The Finite Volume Method*. Pearson Prentice Hall.
52. Wilson KC, Sanders RS, Gillies RG, Shook CA (2010). Verification of the near-wall model for slurry flow. *Powder Technology* 197(3): 247-253.
53. Wilson KC, Sellgren A (2003). Interaction of Particles and Near-Wall Lift in Slurry Pipelines. *Journal of Hydraulic Engineering* 129(1): 73-76.